Scanning Electrochemical Microscopy (SECM): An Investigation of the Effects of Tip Geometry on Amperometric Tip Response

Jonathan L. Amphlett and Guy Denuault*

Department Of Chemistry, University Of Southampton, Highfield, Southampton SO17 1BJ, UK

Received: June 30, 1998; In Final Form: September 16, 1998

Transient and steady-state amperometric tip responses were simulated with an alternating direction implicit algorithm. Compared with previous publications, the simulation domain was designed to account for the diffusion of the redox species around the corner of the insulating sheath. Expanding space and time grids were used to optimize the algorithm, and the simulation was validated by comparison with published data for the microdisk electrode. Tip responses were simulated for a wide range of tip substrate distances over conducting and insulating substrates. The shape of the approach curves was investigated for several electroactive disk to insulator radii ratios. Diffusion around the edge of the insulating sheath was found to have a pronounced effect on the approach curves. In contrast to the findings of earlier studies, tip currents for conducting substrates were found to significantly depend on the tip geometry. The parameters of functions used to describe approach curves in the SECM literature were studied for several tip geometries commonly used experimentally. Simulated results were also used to assess the topographical sensitivity (the rate of change of tip current with respect to tip−substrate distance) and spatial resolution (the ability of the microdisk to distinguish two conducting islands inlaid into an insulating substrate) of the scanning electrochemical microscope (SECM).

Introduction

In this paper, we present a study of the effects of probe geometry on scanning electrochemical microscopy[1,2] experiments. The applications of SECM now include studies of solid−liquid,[3] liquid−liquid,[4] and even liquid−gas[5] interfaces. These new experiments require a range of tip geometries from micropipets[6] with very thin walls to conventional microdisks with large insulating sheaths. In the early days of SECM, Kwak and Bard[7] reported the effect of tip geometry on amperometric tip responses. They showed that the ratio of the insulating glass sheath radius to that of the electroactive disk, R_{glass} (also known as RG) had a strong influence on the Faradaic tip current when the tip was moving in the vicinity of an inert substrate. This effect was explained in terms of the hindered diffusion of a redox mediator from the bulk solution to the tip. They also predicted that the tip current would not be affected by the thickness of the insulating sheath when approaching a conducting material. In this case, the regeneration of the redox mediator by the substrate was found to control the magnitude of the tip current. Mirkin et al.[8] investigated approach curves for conical and hemispherical tips and showed that the dependence of the tip current on the tip−substrate distance could be used to determine the shape of the tip and its characteristic dimensions. Yet most SECM experiments are carried out with inlaid disks made by sealing a cylindrical microwire into an insulating (usually glass) sheath. The electroactive radius ranges from hundreds of nanometers to a few tens of micrometers, while the insulating sheath thickness ranges from a fraction to several multiples of the disk radius. Thus, R_{glass} varies from 1 for a microdisk surrounded with an infinitely small insulating sheath, to infinity for a conventional microdisk used in non-SECM applications. For SECM tips, when it is essential to get close to a substrate, sheath thicknesses on the order of a few electrode radii are used, typically 10. However, Scott and co-workers,[9] for example, used microdisks with an R_{glass} value of 1.25 (an 8 μm carbon fiber diameter coated with a 1 μm thick insulating layer of polyphenylene oxide).

This investigation started because the table of data published by Kwak indicates that the tip current is approximately 5% greater than the theoretical steady-state current to a microdisk electrode in the bulk solution ($i_{tip,\infty} = 4nFDc^b a$ where n, F, D, c^b, and a are respectively the number of electrons, the Faraday constant, the diffusion coefficient, the bulk concentration of the redox species, and the radius of the disk). Up to now, this condition was treated in a manner similar to that used for experimental approach curves, i.e., by normalizing the approach curve with respect to the steady-state current in bulk solution. With this correction, Kwak's data have been extensively used in theoretical and experimental SECM studies, in particular to determine the absolute tip−substrate distance. The authors had suggested that the model could be improved by introducing a more rigorous treatment of the boundary condition at the edge of the insulating sheath.

In this article, we present the results of simulations that expand on the work carried out by Kwak and Bard. The model chosen is constructed around a sophisticated solution domain that includes the tip−substrate gap and the solution around the body of the tip. Thus, it is able to account for the diffusion of the redox mediator around the corner of the insulating sheath. We used the simulation to generate approach curves for several R_{glass} values, and we discuss how the tip current depends on R_{glass} for various positions above the substrate. The simulations were carried out for inert and conducting substrates, and the effect of the R_{glass} values in both cases are presented. The parameters of functions used to describe approach curves in the SECM literature were studied for several tip geometries commonly used experimentally. We also made use of the

10.1021/jp982829u CCC: $15.00
Published on Web 11/11/1998

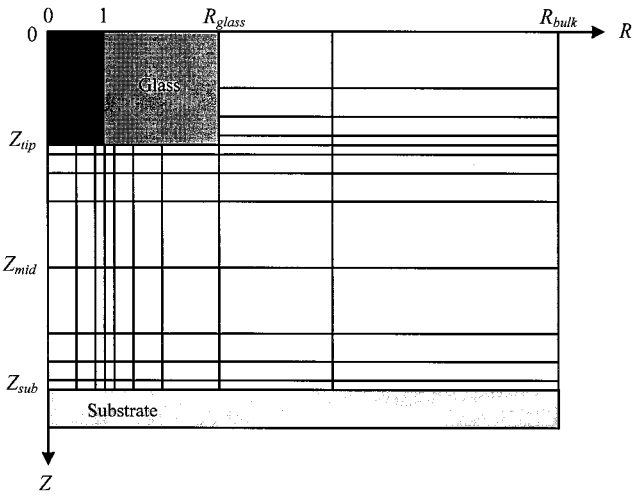

Figure 1. Schematic representation of the two-dimensional simulation domain.

simulated tip currents to investigate the sensitivity of the tip toward topographical changes and discuss the effect of R_{glass} on the spatial resolution during imaging. In particular, we show how spatial resolution is both a function of tip substrate distance and insulating sheath thickness.

Description of the Simulation Model

Much theoretical work has been published on the modeling of chronoamperometric currents for the microdisk electrode. In most cases, the disk was assumed to be embedded into an infinite insulating plane.[10−13] Shoup and Szabo[14] were the first to demonstrate that diffusion from behind the plane of the electrode enhances the flux to the inlaid disk. Their simulation domain allowed accurate simulation of the geometry of the electrode. More recently, Fang and Leddy[15] published the results of a similar study. The work presented here extends the Shoup and Szabo domain to SECM conditions, when the microdisk approaches a substrate.

The domain considers a metal rod sealed in a glass cylinder. The assembly is immersed in the solution of redox mediator and is held at a fixed distance above the substrate. It is assumed that the oxidized and reduced species have the same diffusion coefficient, and for this reason, only one species is included in the simulation. Initially, the simulation domain is set to the bulk concentration of redox mediator everywhere (eqs 1 and 2). At the start of the simulation, the tip potential is stepped from a value where no reaction occurs to one where the tip reaction is diffusion controlled, therefore, the concentration on the disk is set to zero (eq 3). The glass around the disk is insulating, and thus, the flux of redox species is set to zero in the directions perpendicular to the insulating surface (eqs 4 and 5). Where the domain extends to the bulk, the concentration is set to the bulk concentration (eqs 6 and 7). On a conducting substrate (assumed to be connected to a potentiostat), the concentration is set to the bulk value to model the regeneration of the mediator (eq 8a). On an inert substrate, the vertical flux of the species is set to zero to model the absence of electroactivity (eq 8b). The radial flux of the species is set to zero along the symmetry axis (eq 9). Fick's second law in cylindrical coordinates[16] is used to simulate diffusion-controlled mass transport within the domain (eq 10). The conditions and partial differential equation are cast in a dimensionless form on the basis of the variables used by Kwak and Bard[7] ($C = c/c^b$; $R = r/a$; $Z = z/a$; $T = Dt/a^2$) where c, r, z, and t are respectively the concentration of the redox species and the radial, axial, and time coordinates. The complete system of conditions and equation is as follows:

$$T = 0, \quad R_{glass} \le R \le R_{bulk}, \quad 0 \le Z \le Z_{tip}, \quad C = 1 \tag{1}$$

$$T = 0, \quad 0 \le R \le R_{bulk}, \quad Z_{tip} < Z \le Z_{sub}, \quad C = 1 \tag{2}$$

$$T > 0, \quad 0 \le R \le 1, \quad Z = Z_{tip}, \quad C = 0 \tag{3}$$

$$T > 0, \quad 1 < R \le R_{glass}, \quad Z = Z_{tip}, \quad \partial C/\partial Z = 0 \tag{4}$$

$$T > 0, \quad R = R_{glass}, \quad 0 \le Z < Z_{tip}, \quad \partial C/\partial R = 0 \tag{5}$$

$$T > 0, \quad R_{glass} < R \le R_{bulk}, \quad Z = 0, \quad C = 1 \tag{6}$$

$$T > 0, \quad R = R_{bulk}, \quad 0 < Z < Z_{sub}, \quad C = 1 \tag{7}$$

$$T > 0, \quad 0 \le R \le R_{bulk}, \quad Z = Z_{sub}, \quad C = 1 \tag{8a}$$

$$T > 0, \quad 0 \le R \le R_{bulk}, \quad Z = Z_{sub}, \quad \partial C/\partial Z = 0 \tag{8b}$$

$$T > 0, \quad R = 0, \quad Z_{tip} < Z < Z_{sub}, \quad \partial C/\partial R = 0 \tag{9}$$

$$\frac{\partial C}{\partial T} = \frac{\partial^2 C}{\partial R^2} + \frac{1}{R}\frac{\partial C}{\partial R} + \frac{\partial^2 C}{\partial Z^2} \tag{10}$$

The subscripts tip, glass, bulk, and sub respectively refer to the tip surface, the insulating glass sheath surface, the bulk solution away from the tip, and the substrate surface. The normalized tip−substrate distance, known as d/a, is therefore equal to $Z_{sub} - Z_{tip}$. The dimensionless tip current was calculated as follows

$$\frac{i_{tip}}{4nFDc^b a} = \frac{\pi}{2}\int_0^1 \left.\frac{\partial C}{\partial Z}\right|_{Z_{tip}} R\,\mathrm{d}R \tag{11}$$

where, as usual in SECM treatment, the tip current has been normalized with respect to the steady-state current to an inlaid disk electrode.

Fang and Leddy[15] used the explicit finite difference (EFD) method to simulate diffusion around the microdisk glass edge. While EFD is simple to implement, it becomes unstable when the time step is too large relative to the grid size.[17,18] This means that long accurate simulations involving fine grids take huge amounts of computation time. To remove the limit on time step we solved the system of conditions (eqs 1−9) and eq 10 with a finite difference alternating-direction implicit (ADI) scheme. This algorithm, introduced by Peaceman and Rachford[19] in 1955, is effectively a two-dimensional version of the Crank−Nicholson[20] scheme proposed in 1947. It has previously been used to simulate diffusion to microdisk electrodes[12,21] and SECM tips.[22−27] This scheme was chosen because it eliminates the restriction on time steps, permits the use of optimized space grids, facilitates the treatment of implicit boundary conditions, and allows long simulations necessary to reach near steady-state conditions.

To focus concentration points in areas of high flux, the domain was discretized with an exponentially expanding space grid (EESG) as first implemented by Joslin and Pletcher[28] and since used in many SECM simulations.[7,22−27] Figure 1 illustrates the regions of the domain where the mesh focused the concentration points. The transformations used along R and Z are based upon Feldberg's transform[29] and are described below

$$0 \le R < 1, \quad X = n_{disk}\Delta X - \ln[1 + A(1 - R)] \tag{12}$$

$$1 \le R < R_{bulk}, \quad X = n_{disk}\Delta X + \ln[1 + A(R - 1)] \quad (13)$$

$$0 \le Z < Z_{tip}, \quad Y = n_{tip}\Delta Y - \ln[1 + A(Z_{tip} - Z)] \quad (14)$$

$$Z_{tip} \le Z < Z_{mid}, \quad Y = n_{tip}\Delta Y + \ln[1 + A(Z - Z_{tip})] \quad (15)$$

$$Z_{mid} \le Z \le Z_{sub}, \quad Y = (n_{tip-sub} + n_{tip})\Delta Y - \ln[1 + B(Z_{sub} - Z)] \quad (16)$$

where Z_{tip}, Z_{mid}, Z_{sub}, and R_{bulk} are coordinates defined in Figure 1. n_{disk}, n_{tip}, and $n_{tip-sub}$ are respectively the number of points along the disk, behind the plane of the electrode, and between the tip and the substrate. X and Y are the coordinates which define the equally spaced grid to be transformed, while ΔX and ΔY determine the overall density of concentration points. In the radial direction, concentration points are focused around the boundary of the microdisk and its insulating surrounding. In the axial direction, concentration points are focused at the surfaces of both the substrate and the microdisk assembly. A and B are the expansion grid coefficients. For a small number of concentration points, the accuracy of the tip current depends heavily on these expansion coefficients. However, the dependency of tip current on A and B decreases dramatically as the density of the mesh increases. For this work, the grid density was such (50 points across the surface of the disk) that the choice of expansion coefficient was almost arbitrary. The value of A was set to 2.0 simply because it gives the most accurate transient response with respect to the analytical data of Aoki and Osteryoung.[30] B was chosen to make the tip−substrate distance exact and was typically in the range 1.9−2.1. In all the simulations, Z_{tip} and the distance between R_{bulk} and R_{glass} were set to 400; above these values, the first eight decimals of the simulated tip current were found to be constant.

To further increase the efficiency, an expanding time-stepping procedure was included in the algorithm. Small time steps are necessary at the start of the simulation to model large fluxes of redox mediator near the microdisk. On the other hand, changes in concentration profiles are very small when the system approaches a steady state and time steps can be increased to save computer time. Various methods can be used to expand the time steps, but they are usually based on the same principles as those for the expanding space grid. The method used here was simply to increase the time step size linearly with dimensionless time according to eq 17

$$\Delta T = (T + 1)\Delta T_0 \quad (17)$$

where ΔT is the expanding time step and ΔT_0 is the initial time step.

The validity and accuracy of the simulations were assessed by comparing the transient tip response for an inlaid ($R_{glass} \rightarrow \infty$) microdisk located in the bulk ($d/a \rightarrow \infty$) with the analytical solutions at short and long times proposed by Aoki and Osteryoung.[13] In both cases, the simulation was found to reach an accuracy of ca. 0.5%, a value well below the range of common experimental errors. Transients were also compared to the equation proposed by Shoup and Szabo[10]. After validation, the same A and n_{disk} values were used for all the simulations. The other parameters were modified to reflect new domain geometries but did not affect the accuracy of the simulation.

Results and Discussion

Influence of R_{glass} on Approach Curves. Fang and Leddy[15] confirmed the results of Shoup and Szabo[10] who showed that the steady-state current to a microdisk electrode significantly increases when the insulating sheath thickness is reduced. This is a consequence of the greater availability of reactant diffusing from behind the plane of the electrode. Figure 2 illustrates that our model emulates these results when the tip−substrate distance is large. The agreement with Shoup and Szabo's data at smaller R_{glass} values is very good, but the values by Fang and Leddy appear to be slightly too large. When $R_{glass} = 1000$, the steady-state dimensionless tip current is 1.005, indicating that the tip is behaving as a disk inlaid in an infinitely large insulator. Quantitatively, the simulation demonstrates that the steady-state current to a microdisk can be at least 40% greater than the theoretical $4nFDc^b a$ value when the insulating sheath thickness tends toward zero. In principle, if the microdisk radius, the diffusion coefficient, and the concentration are known, then an estimate of the effective R_{glass} value can be obtained from the relationship shown in Figure 2. For example, a microelectrode with an R_{glass} of 2 should show an increase over the theoretical steady-state current of approximately 10%. However, this would require a very careful experimental procedure such as thermostatic control to avoid any variation in D.

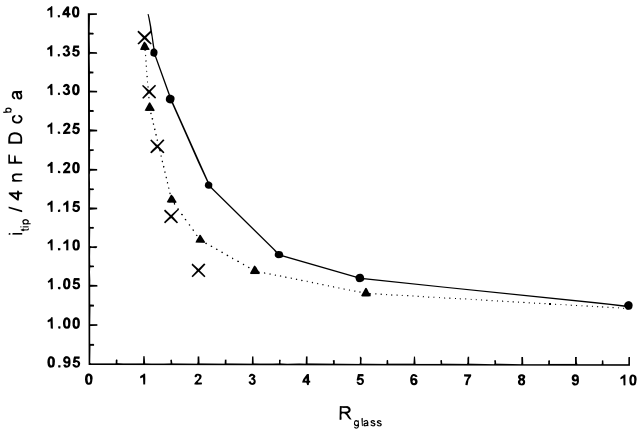

Figure 2. Plot of the steady-state dimensionless tip current against the dimensionless insulating sheath radius, $d/a = 400$: (▲) this work, (×) Shoup and Szabo,[10] (●) Fang and Leddy.[15]

Many simulations assume an infinitely thick insulating sheath surrounding the microdisk and do not consider the edge of the glass. Figure 2 shows that the error due to this assumption is experimentally significant when R_{glass} is less than 5 (assuming that experimental measurements can be made with a 5% accuracy). In the worst case, this assumption could underestimate the steady-state tip currents by up to 40%.

The remainder of this section discusses how the thickness of the insulator affects the current when the electrode travels toward a sample surface in an SECM experiment. Just as in the original paper by Kwak and Bard,[7] a plot of steady-state tip current is produced for electrodes with different R_{glass} values over a range of tip−substrate distances. Simulated approach curves to both conducting and insulating substrates are shown in Figure 3. To facilitate comparison between approach curves, tip currents were normalized with respect to their individual bulk steady-state values shown in Figure 2, as they would be experimentally. Figure 3 shows how the shape of predicted approach curves is heavily dependent on tip geometry, especially when approaching an insulating substrate. The higher availability of redox mediator to low R_{glass} electrodes affects the diffusion field within the tip−substrate gap. As the microdisk approaches an insulating substrate, the difference between high and low R_{glass} electrodes is enhanced. These results are basically in agreement with Kwak's data. However, in contrast to Kwak's data, the

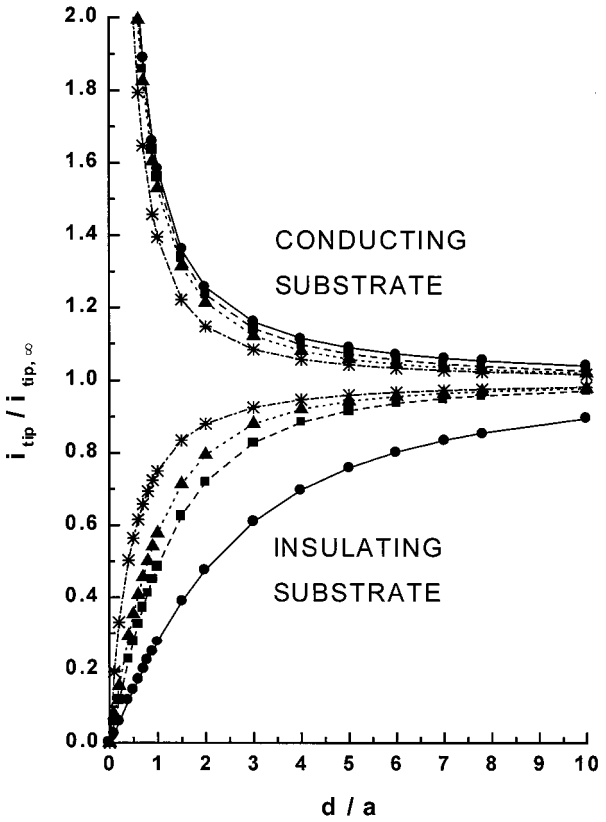

Figure 3. Simulated dimensionless approach curves toward conducting (top curves) and insulating (bottom curves) substrates: R_{glass} = (●) 1000, (■) 10, (▲) 5, (*) 1.5. For each curve, the currents are normalized with respect to the steady-state current in the bulk for the particular R_{glass} value.

present simulation shows that, even for positive feedback, the difference between high and low R_{glass} electrodes is significant. This difference is even more apparent when the approach curves are not normalized with respect to the individual bulk current values because R_{glass} affects both the shape of the curves and the magnitude of the current.

It is clear from the above discussion that fits based on simulated data should therefore use the appropriate approach curve for the SECM microdisk geometry being used. This is true not only for hindered diffusion but also for positive feedback. To facilitate further use of the results, we have fitted our simulated current−distance plots to analytical approximations used to describe approach curves to conducting and insulating substrates.[8] For a current−distance curve controlled by hindered diffusion we fitted eq 18,

$$\frac{i_{tip}}{i_{tip,\infty}} = \frac{1}{\left[k_1 + \left(\frac{k_2}{L}\right) + k_3 \exp\left(\frac{k_4}{L}\right)\right]} \qquad (18)$$

where i_{tip} and $i_{tip,\infty}$ are respectively the tip current at a given tip−substrate distance d and in the bulk, k_1, k_2, k_3 and k_4 are constants which depend on R_{glass} and L stands for d/a, the dimensionless tip−substrate distance. While for a current-distance curve controlled by positive feedback we fitted eq 19

$$\frac{i_{tip}}{i_{tip,\infty}} = k_1 + \left(\frac{k_2}{L}\right) + k_3 \exp\left(\frac{k_4}{L}\right) \qquad (19)$$

Table 1 shows how the four coefficients change with R_{glass}. For comparison, the values previously reported[8] for R_{glass} = 10 are included. The validity of the coefficients is given in terms of the range of tip−substrate distances where the fit between the equation and the simulated approach curve is better than 1%. Except for R_{glass} = 1.11, the smooth dependence of k_1, k_2, k_3, and k_4 on R_{glass} means that the shape of approach curves for electrode geometries not listed in Table 1 can be interpolated from bracketing k values. The coefficients given in Table 1 can be used for tip−substrate distances outside the validity range, but the percentage error is typically 2 or 3%. With equations (18 and 19) and Table 1, users can fit their experimental approach curves to the analytical approach curves appropriate to their tip geometry.

TABLE 1: R_{glass} Dependence of the Coefficients k_1, k_2, k_3, and k_4 in eq 18 for an Approach Curve under Hindered Diffusion Control and in eq 19 for an Approach Curve Controlled by Positive Feedback[a]

R_{glass}	k_1	k_2	k_3	k_4	% error	L validity range
			Hindered Diffusion (eq 18)			
1002	0.13219	3.37167	0.8218	−2.34719	<1%	0.3−20
100	0.27997	3.05419	0.68612	−2.7596	<1%	0.4−20
50.9	0.30512	2.6208	0.66724	−2.6698	<1%	0.4−20
20.1	0.35541	2.0259	0.62832	−2.55622	<1%	0.4−20
15.2	0.37377	1.85113	0.61385	−2.49554	<1%	0.4−20
10.2	0.40472	1.60185	0.58819	−2.37294	<1%	0.4−20
8.13	0.42676	1.46081	0.56874	−2.28548	<1%	0.4−20
5.09	0.48678	1.17706	0.51241	−2.07873	<1%	0.2−20
3.04	0.60478	0.86083	0.39569	−1.89455	<0.2%	0.2−20
2.03	0.76179	0.60983	0.23866	−2.03267	<0.15%	0.2−20
1.51	0.90404	0.42761	0.09743	−3.23064	<0.7%	0.2−20
1.11	−1.46539	0.27293	2.45648	8.995E-7	<1%	2−20
10 from ref 8	0.292	1.151	0.6553	−2.4035	<1.2%	0.05−20
			Positive Feedback (eq 19)			
1002	0.7314	0.77957	0.26298	−1.29077	<0.2%	0.1−200
10.2	0.72627	0.76651	0.26015	−1.41332	<0.3%	0.1−200
5.1	0.72035	0.75128	0.26651	−1.62091	<0.5%	0.1−20
1.51	0.63349	0.67476	0.36509	−1.42897	<0.2%	0.1−200
10 from ref 8	0.68	0.78377	0.3315	−1.0672	<0.7%	0.05−20

[a] The last two columns give the maximum relative error between the equation and the simulated current−distance curve and the range of tip−substrate distances over which these errors hold. Values reported by Mirkin et al.[8] are also included.

The results shown in Figures 2 and 3 indicate a unique relationship between the tip current, the insulating sheath thickness, and the tip−substrate distance. Notably, the current recorded when the tip travels toward an inert substrate is strongly influenced by R_{glass}. In principle, this relationship could be used to determine experimentally the value of R_{glass}. The procedure should work well since both the magnitude of the current and the shape of the current−distance curve depend on R_{glass}. However, the simulation suggests that distinguishing R_{glass} values higher than 10 would be difficult since neither the limiting current in the bulk nor the approach curve strongly depend on the insulator thickness.

Influence of R_{glass} on SECM Imaging. Another observation can be made from Figure 3. The topographical sensitivity of the microelectrode (i.e., how sensitive the electrode is to small changes in tip−substrate distance) can be perceived by considering the derivative of the approach curves. A high rate of change of tip current with respect to tip−substrate distance means that the microelectrode will be able to detect small topographical features on the substrate. Clearly, this is advantageous if the microelectrode is being used for imaging. Figure

3 shows that at the tip−substrate distances typically used for SECM mapping, $d/a < 2$, electrodes with low R_{glass} values have the highest sensitivity to topographical changes.

However, the main advantage of using the SECM is not in topographic mapping but in the fact that it can probe variations in surface reactivity. Thus, it is interesting to investigate how the spatial resolution depends on the tip geometry. We define the spatial resolution of the SECM as the ability of the microelectrode tip to resolve two small conducting islands close together, inlaid into an insulating substrate.

The simulation was modified to investigate the influence of tip geometry on the tip ability to detect variations in the nature of the substrate. A conducting island (assumed to be connected to a potentiostat) was included in the substrate and steady-state concentration distributions and flux contours were simulated for a range of insulator thicknesses. Analysis of the flux lines at a d/a value of 1, showed that larger R_{glass} electrodes were more sensitive to the presence of conducting islands on the substrate. However, as a result of the cylindrical symmetry of the domain, the simulation only predicts the influence of the tip geometry on the magnitude of the tip response. The study of spatial resolution requires the simulation of a line scan and the implementation of a moving boundary to reflect the movement of the tip with respect to the substrate. Unfortunately, simulating the scan of a microelectrode across a substrate containing conducting islands destroys the symmetry of the grid shown in Figure 1. Ideally, a three-dimensional simulation should be used; however, the high computational overheads required makes this kind of simulation prohibitively time-consuming. Instead, a two-dimensional simulation was carried out using a domain based upon the one shown in Figure 1 but doubled in size to reflect concentrations in front of and behind the tip. The diffusion equation was solved in planar coordinates with appropriate initial and boundary conditions. Simulations were allowed to reach a steady state; then, to simulate the line scan, two conducting islands were made to travel along the lower boundary of the domain. The islands were assumed to be connected to a potentiostat to promote positive feedback with the tip.

The results of this simulation are purely qualitative as we are in effect simulating an infinitely long microband electrode passing a pair of infinitely long conducting strips, inlaid into an insulating plane. Although no real current can be derived from such a procedure, we can obtain a qualitative measure of the tip current magnitude by considering the total two-dimensional flux to the electrode at any one time. The algorithm is thought to be adequate since the objective is simply to compare the responses of tips with different insulating thicknesses.

The results shown in Figure 4 were simulated with the following conditions. The tip−substrate distance, d/a, was set to 1, the width of the islands to $a/2$, and the distance between them to $4a$. For each line scan, the baseline, i.e., the steady-state current due to hindered diffusion, was subtracted. In agreement with the results shown in Figure 2, the baseline is greater for small R_{glass} electrodes and the subtraction reveals the spatial resolution. When $R_{glass} = 2$, the minimum between the two peaks is lower than when $R_{glass} = 10$; moreover, the base of the peaks is narrower when using a smaller insulating sheath. Thus, the plot demonstrates that a microdisk with a small insulating sheath ($R_{glass} = 2$) is better able to resolve the two conducting islands. The presence of the conducting islands produces a greater increase in tip current for the microelectrode with the larger sheath thickness ($R_{glass} = 10$). This result is in accordance with that obtained for a single island in the *axy*-symmetrical simulation. A larger sheath thickness therefore increases the sensitivity of a microelectrode while decreasing its resolution.

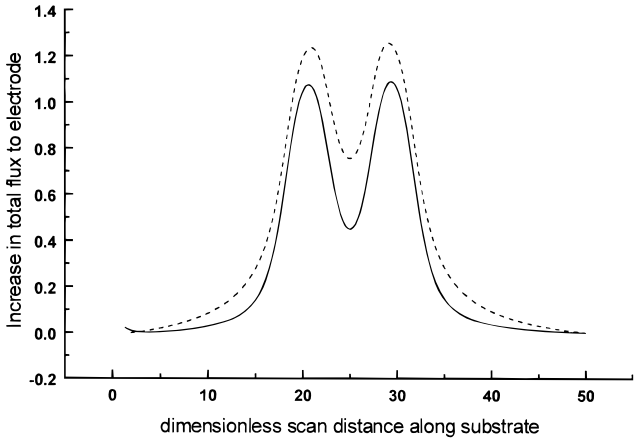

Figure 4. Simulated tip current line scans for two conducting islands: dashed line, $R_{glass} = 10$; solid line, $R_{glass} = 2$. The tip−substrate distance, d/a, was set to 1, the width of the islands to $a/2$, and the distance between them to $4a$. For each line scan, the baseline, i.e., the steady-state current due to hindered diffusion, was subtracted.

The resolution of the SECM also depends on the tip−substrate distance. As d/a increases, the amount of feedback current produced by the conducting islands decreases and the tip is less able to resolve the features. However, a proper quantitative treatment of the combined effects of *RG* and d/a on imaging resolution would require a three-dimensional simulation.

Conclusion

Transient and steady-state amperometric tip responses were simulated with an alternating direction implicit algorithm implementing expanding space and time grids. The simulation domain was designed to account for the diffusion of the redox species around the corner of the insulating sheath. We show that diffusion round the edge of the insulating sheath has a pronounced effect on the approach curves, not only under hindered diffusion control but also under positive feedback diffusion control. The parameters of functions used to describe approach curves in the SECM literature are tabulated for several tip geometries commonly used experimentally. The functions can be fitted to experimental approach curves in order to determine the absolute tip−substrate distance.

The study of spatial resolution presented here is directly applicable to the investigations carried out by White et al.[31−33] where a microelectrode is used to map electroactive sites on a flat insulating oxide. The microdisks used by White and co-workers have very thin insulating sheaths. Our simulations show that their tips are better able to image the true dimensions of the conducting regions, but as a consequence, they are less sensitive to smaller substrate features. Although the results obtained are purely qualitative, we expect that a true three-dimensional simulation would confirm the observations made and in fact show an even greater effect from the insulator thickness as the shielding applies in all radial directions.

Acknowledgment. The authors acknowledge the support of the EPSRC (Grant GR/K14704, studentship for J.L.A.) and John Angus for helpful discussions on the expanding grid.

References and Notes

(1) Bard, A. J.; Denuault, G.; Lee, C.; Mandler, D.; Wipf, D. O. *Acc. Chem. Res.* **1990**, *23*, 357.

(2) Bard, A. J.; Fan, F.-R F.; Mirkin, M. V. *Electroanal. Chem.* **1994**, *18*, 243.
(3) Unwin, P. R.; Bard A. J. *J. Phys. Chem.* **1992**, *96*, 5035.
(4) Shao, Y. H.; Mirkin, M. V. *J. Electroanal. Chem.* **1997**, *439*, 137.
(5) Slevin, C. J.; Macpherson, J. V.; Unwin, P. R. *J. Phys. Chem. B* **1997**, *101*, 10851.
(6) Shao, Y.; Mirkin, M. V. *Natl. Meet.—J. Electrochem. Soc.* **1998**, *193*, Abstract 983.
(7) Kwak, J.; Bard, A. J. *Anal. Chem.* **1989**, *61*, 1221.
(8) Mirkin, M. V.; Fan, F.-R. F.; Bard, A. J. *J. Electroanal. Chem.* **1992**, *328*, 47.
(9) Scott, E. R.; White, H. S.; Phipps, J. B. *Solid State Ionics* **1992**, *53−56*, 176.
(10) Shoup, D.; Szabo, A. *J. Electroanal. Chem.* **1982**, *140*, 237.
(11) Shoup, D.; Szabo, A. *J. Electroanal. Chem.* **1984**, *160*, 1.
(12) Heinze, J. *J. Electroanal. Chem.* **1981**, *124*, 73.
(13) Aoki, K.; Osteryoung, J. *J. Electroanal. Chem.* **1981**, *122*, 19.
(14) Shoup, D.; Szabo, A. *J. Electroanal. Chem.* **1984**, *160*, 27.
(15) Fang, Y.; Leddy, J. *Anal. Chem.* **1995**, *67*, 1259.
(16) Bard, A. J.; Faulkner, L. R. *Electrochemical Methods, Fundamentals and Applications*; Wiley: New York, 1980.
(17) Britz, D. *Digital Simulation In Electrochemistry*, 2nd revised and extended ed.; Springer-Verlag: Berlin, 1988.
(18) Speiser, B. *Electroanal. Chem.* **1996**, *19*, 1.
(19) Peaceman, D. W.; Rachford, H. H. *J. Soc. Ind. Appl. Math.* **1995**, *3*, 28.
(20) Crank, J.; Nicholson, P. *Proc. Cambridge Philos. Soc.* **1947**, *43*, 50.
(21) Taylor, G.; Girault, H. H. *J. Electroanal. Chem.* **1990**, *293*, 19.
(22) Unwin, P. R.; Bard, A. J. *J. Phys. Chem.* **1991**, *96*, 7814.
(23) Pierce, A.; Unwin, P. R.; Bard, A. J. *Anal. Chem.* **1992**, *64*, 1795.
(24) Unwin, P. R.; Mirkin, M. V.; Bard, A. J. *J. Phys. Chem.* **1992**, *96*, 4917.
(25) Zhou, F.; Unwin, P. R.; Bard, A. J. *J. Phys. Chem.* **1991**, *96*, 7814.
(26) Unwin, P. R.; Bard, A. J. *J. Phys. Chem.* **1991**, *96*, 5035.
(27) Demaile, C.; Unwin, P. R.; Bard, A. J. *J. Phys. Chem.* **1996**, *100*, 14137.
(28) Joslin, T.; Pletcher, D. *J. Electroanal. Chem.* **1974**, *49*, 171.
(29) Feldberg, S. W. *J. Electroanal. Chem.* **1981**, *127*, 1.
(30) Aoki, K.; Osteryoung, J. *J. Electroanal. Chem.* **1984**, *160*, 335.
(31) White, H. S.; Casillas, N.; Charlebois, S. J.; Smyrl, W. H. *J. Electrochem. Soc.* **1993**, *140*, 142.
(32) White, H. S.; Casillas, N.; Charlebois, S. J.; Smyrl, W. H. *J. Electrochem. Soc.* **1994**, *141*, 636.
(33) White, H. S.; Basame, S. B. *J. Phys. Chem.* **1995**, *99*, 16430.